Diffusing acoustic wave spectroscopy

M. L. Cowan,[1] I. P. Jones,[1,*] J. H. Page,[1,2,†] and D. A. Weitz[2]
[1]*Department of Physics and Astronomy, University of Manitoba, Winnipeg, Manitoba, Canada R3T 2N2*
[2]*Department of Physics and DEAS, Harvard University, Cambridge, Massachusetts 02138*
(Received 5 December 2001; published 12 June 2002)

We have developed a technique in ultrasonic correlation spectroscopy called diffusing acoustic wave spectroscopy (DAWS). In this technique, the motion of the scatterers (e.g., particles or inclusions) is determined from the temporal fluctuations of multiply scattered sound. In DAWS, the propagation of multiply scattered sound is described using the diffusion approximation, which allows the autocorrelation function of the temporal field fluctuations to be related to the dynamics of the multiply scattering medium. The expressions relating the temporal field autocorrelation function to the motion of the scatterers are derived, focusing on the types of correlated motions that are most likely to be encountered in acoustic measurements. The power of this technique is illustrated with ultrasonic data on fluidized suspensions of particles, where DAWS provides a sensitive measure of the local relative velocity and strain rate of the suspended particles over a wide range of time and length scales. In addition, when combined with the measurements of the rms velocity of the particles using dynamic sound scattering, we show that DAWS can be used to determine the spatial extent of the correlations in the particle velocities, thus indirectly measuring the particle velocity correlation function. Potential applications of diffusing acoustic wave spectroscopy are quite far reaching, ranging from the ultrasonic nondestructive evaluation of the dynamics of inhomogeneous materials to geophysical studies of mesoscopic phenomena in seismology.

DOI: 10.1103/PhysRevE.65.066605 PACS number(s): 43.35.+d, 43.20.+g, 43.90.+v, 82.70.Kj

I. INTRODUCTION

The scattering of ultrasonic waves, especially from objects buried inside optically opaque materials, has been used extensively to image internal structures in inhomogeneous media and to probe their physical properties [1]. For example, many applications have been demonstrated in both acoustic microscopy [2] and medical imaging, ranging from three-dimensional visualizations of subsurface details in carbon nanotubes to images of fetuses and blood flow in human beings [3]. However, these methods break down in materials where strong multiple scattering occurs, since multiple scattering scrambles the directions in which the waves are traveling and exact information on the location of the scattering objects is lost. In this case, images of the scattered wave field are dominated by acoustic speckle, which arises from the interference between the scattered waves that have traveled different multiple scattering paths through the sample. Thus, speckles can completely obscure static images of the scatterers, and different approaches are needed to extract meaningful information from the scattered waves. One such approach is to use the fluctuations that occur in the speckle pattern when the scatterers are moving to investigate the system's dynamics. This is the approach followed in this paper, where we describe an ultrasonic technique, called diffusing acoustic wave spectroscopy (DAWS), and demonstrate its potential for investigating the dynamics of strongly scattering media over a wide range of time and length scales. While brief accounts of the technique have been published previously [4–6], the aim of this paper is to give a sufficiently complete description of DAWS to facilitate its practical implementation in a wide range of possible applications.

Diffusing acoustic wave spectroscopy determines the dynamics of strongly scattering media from the temporal fluctuations of ultrasonic waves that are scattered many times before leaving the sample. This technique is made feasible by recent progress in understanding the diffusion of multiply scattered ultrasonic waves, an approach that we have shown to be extremely powerful and remarkably accurate for describing acoustic wave transport under these conditions [7,8]. By modeling the ultrasound propagation using the diffusion approximation, we show how this technique determines the relative motion of the scatterers from the autocorrelation function of the field fluctuations. Since multiply scattered sound is used, each scatterer need move only a minute fraction of a wavelength for its motion to be detected, giving extremely high sensitivity to small displacements of the scatterers. This technique is analogous to diffusing wave spectroscopy (DWS) using light [9,10], which has been used to study a wide range of systems and physical phenomena, ranging from particle sizing to measurements of particle motion on angstrom length scales, and from the aging of foams to high frequency rheology [11,12]. However, the motion of wavelength-sized particles in ultrasonics is generally quite different from that measured using light, necessitating a careful examination of the correlation function from which the particle dynamics are determined. The experimental approach is also different, largely because of the relative ease with which pulsed measurements can be performed in ultrasonics, an approach that leads to a significant simplification in the measurement of particle dynamics from the temporal correlation function. We illustrate the feasibility of DAWS

*Present address: FNC Inc., 606 Van Buren Ave., Oxford, MS 38655.
†Author to whom correspondence should be addressed. Electronic address: jhpage@cc.umanitoba.ca

by showing how it can be used to measure the relative mean square displacement and local strain rate of fluidized suspensions of particles, where this technique has recently led to valuable insights into their complex flow behavior [4].

The outline of this paper is as follows. In Sec. II, we derive the relationship between the field autocorrelation function that is measured experimentally and the relative mean square displacement of the scattering particles. The temporal evolution of the relative mean square displacement is described in systems with partially correlated particle flows, and the approximate relationship between the local relative velocity and strain rate is discussed. Since it is usually best to perform diffusing acoustic wave spectroscopy measurements in pulsed mode, the main emphasis is on pulsed DAWS, although the autocorrelation function for continuous-wave (cw) DAWS is also presented. Section III describes how DAWS experiments are performed. The minimum multiple scattering path length required for accurate DAWS measurements is determined, and the results of pulsed and cw DAWS are compared to illustrate the relative advantages of the two approaches. In Sec. IV, representative data for the experiments performed on fluidized suspensions of particles are presented in order to illustrate the considerable range of dynamic information that can be obtained using DAWS. Our main conclusions are stated in Sec. V.

II. THEORY

In diffusing acoustic wave spectroscopy, it is the temporal fluctuations of the multiply scattered pressure field $\psi(t)$ that are measured experimentally, and the motion of the scattering particles can be determined directly from the field autocorrelation function,

$$g_1(\tau)=\frac{\int \psi(t)\psi^*(t+\tau)dt}{\int |\psi(t)|^2 dt}. \tag{1}$$

To calculate $g_1(\tau)$, we model the propagation of ultrasound through the material using the diffusion approximation, in which the multiply scattered ultrasonic waves travel through the sample in a random-walk process characterized by the transport mean free path l^*, the energy velocity v_e, and the diffusion coefficient $D=v_e l^*/3$. In what follows, we will discuss the transmission geometry in which the generator and detector are on opposite sides of the sample, although the method can be readily extended to treat the reflection geometry as well. For the ultrasonic experiments described below, the scattering is almost isotropic on average, so that $l^* \cong l_s \equiv l$, where l_s is the scattering mean free path. We begin with the isotropic scattering case by considering a single random-walk path of n steps through the sample having total length $s=(n+1)l$ [13]. This path's contribution to the decay of $g_1(\tau)$ is determined by the total phase change resulting from the motion of all the scatterers in the path. From Fig. 1, it is clear that this phase change can be written as

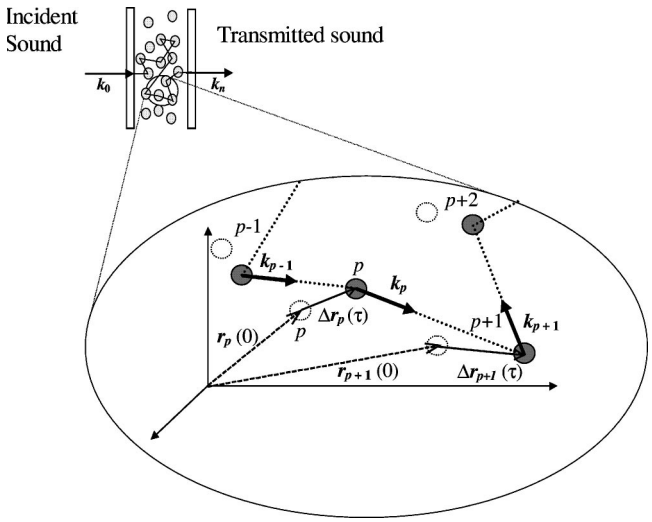

FIG. 1. Segment of a multiple scattering path with moving scatterers. Solid spheres are at $t=\tau$, open spheres are at $t=0$.

$$\Delta\phi^{(n)}(\tau)=\sum_{p=0}^{n}\Delta\phi_p(\tau)=\sum_{p=0}^{n}[\vec{k}_p\cdot\{\Delta\vec{r}_{p+1}(\tau)-\Delta\vec{r}_p(\tau)\}]$$
$$=\sum_{p=1}^{n-1}\vec{k}_p\cdot\Delta\vec{r}_{\mathrm{rel},p}(\tau,l)+[\vec{k}_0\cdot\Delta\vec{r}_1(\tau)-\vec{k}_n\cdot\Delta\vec{r}_n(\tau)], \tag{2}$$

where $\vec{k}_p$ is the wave vector of the wave scattered from the pth to the $(p+1)$th particle, and $\Delta\vec{r}_{\mathrm{rel},p}(\tau)=\Delta\vec{r}_{p+1}(\tau)-\Delta\vec{r}_p(\tau)$ is their relative displacement during the time interval τ. The last two terms represent the motion of the first and last scatterer relative to the source ($p=0$ term) and detector ($p=n$ term), respectively; for large n their contribution is small and can be neglected. By definition, the average distance between particles in the scattering path is given by $\langle|\vec{r}_{p+1}-\vec{r}_p|\rangle=l$. The phase change $\Delta\phi^{(n)}(\tau)$ can also be written in terms of the scattering wave vector $\vec{q}_p=\vec{k}_p-\vec{k}_{p-1}$ as $\Delta\phi^{(n)}(\tau)=\Sigma_{p=1}^{n}\vec{q}_p\cdot\Delta\vec{r}_p(\tau)$, but this commonly used form in DWS is not appropriate when the motion of adjacent scatterers in the path is correlated, as is likely to occur for the large millimeter-sized particles that scatter ultrasonic waves strongly. The total field autocorrelation function is obtained by averaging over all paths with n events and summing over all path lengths (i.e., all n) that contribute to the total field measured at the detector, giving

$$g_1(\tau)=\sum_n g_1^n(\tau)=\sum_n P(n)\langle e^{-i\Delta\phi^{(n)}(\tau)}\rangle. \tag{3}$$

Here the factor $P(n)\equiv\langle|\psi^{(n)}(0)|^2\rangle/\langle|\psi^2|\rangle$ is the fraction of the total scattered sound intensity in paths having n scattering events. In a continuous-wave experiment, the summation in Eq. (3) extends over all n. However, in a pulsed experiment, the average path length s is selected by measuring the field fluctuations at a fixed sampling time $t_s=s/v_e$ after the input pulse is incident on the sample, and the summation is

restricted to include only those paths whose length differs from the average by the pulse width $(\Delta t/v_e)$. In particular, for a narrow pulse, $P(n)$ is essentially constant in the summation over n and the normalized field correlation function takes on the relatively simple form

$$g_1(\tau) \simeq \langle e^{-i\,\Delta\phi^{(n)}(\tau)} \rangle. \tag{4}$$

Equation (4) shows immediately one of the great advantages of pulsed measurements, namely, that $g_1(\tau)$ does not depend on the effects of boundary conditions or absorption in the diffusive propagation of ultrasound through the sample.

For large n it is a good approximation to assume that the successive phase shifts $\Delta\phi_p(\tau)$ in Eq. (2) are uncorrelated. Then Eq. (4) becomes

$$g_1(\tau) \simeq \langle e^{-i\,\vec{k}\cdot\Delta\vec{r}_{\rm rel}(\tau,l)} \rangle^{n-1} \langle e^{i\vec{k}\cdot\Delta\vec{r}_{\rm rel}(\tau,R)} \rangle, \tag{5}$$

where the second term gives the contribution from the relative motion of the first and last particles in the scattering path, which are separated by a distance R. In a transmission experiment, $R \sim L$, where L is the sample thickness. Equation (5) can be further simplified to

$$g_1(\tau) \simeq \exp\left[-\frac{n}{2} \langle [\vec{k}\cdot\Delta\vec{r}_{\rm rel}(\tau,l)]^2 \rangle \right] \times \exp\left[-\frac{1}{2} \{ \langle [\vec{k}\cdot\Delta\vec{r}_{\rm rel}(\tau,R)]^2 \rangle - \langle [\vec{k}\cdot\Delta\vec{r}_{\rm rel}(\tau,l)]^2 \rangle \} \right], \tag{6}$$

where we have used a cumulant expansion, retaining only the leading nonvanishing term, which is the second cumulant $\langle [\vec{k}\cdot\Delta\vec{r}_{\rm rel}(\tau)]^2 \rangle$. Higher-order terms in the cumulant expansion are negligible since, for the range of times over which $g_1(\tau)$ can be reliably measured, the phase fluctuations are small for any step along any path having large n. In Eq. (6), $\langle \cdots \rangle$ denotes both a configurational average over the change in position of the scatterers and an average over all possible wave vectors $\vec{k}_p$. When the directions of $\vec{k}$ and $\Delta\vec{r}_{\rm rel}$ are not correlated, the average in Eq. (6) is easy to perform, giving

$$g_1(\tau) \simeq \exp\left[-\frac{nk^2}{6} \left(\langle \Delta r_{\rm rel}^2(\tau,l) \rangle + \frac{1}{n} \{ \langle \Delta r_{\rm rel}^2(\tau,R) \rangle - \langle \Delta r_{\rm rel}^2(\tau,l) \rangle \} \right) \right]. \tag{7}$$

The term in curly brackets will be zero if the motion of particles is uncorrelated for all distances greater than or equal to l, since then $\langle \Delta r_{\rm rel}^2(\tau,R) \rangle = \langle \Delta r_{\rm rel}^2(\tau,l) \rangle$. Furthermore, in this case of uncorrelated motion, $\langle \Delta r_{\rm rel}^2(\tau,l) \rangle$ is twice the single-particle mean square displacement $\langle \Delta r^2(\tau) \rangle$, leading to the form often used in DWS for diffusive motion [9,10]. However, even when this condition is not satisfied, the term in curly brackets in Eq. (7) at most gives a contribution that is of order $1/n$ times smaller than the first term and can be neglected for large enough n, giving, to a good approximation, the simple relation

$$g_1(\tau) \simeq \exp\left[-\frac{nk^2}{6} \langle \Delta r_{\rm rel}^2(\tau,l) \rangle \right]. \tag{8}$$

Here, in a pulsed experiment, n is determined by the path length and is directly related to the amount of time that the ultrasonic waves have spent traveling through the sample.

When the directions of the wave vector and relative mean square displacement are correlated, the average magnitude of $\Delta\vec{r}_{{\rm rel},p}(\tau,l)$ projected along the wave vector $\vec{k}_p$ depends on the angle θ_p between $\Delta\vec{r}_{{\rm rel},p}(\tau,l)$ and $\vec{k}_p$. As a result, the average of $\langle (\vec{k}_p\cdot\Delta\vec{r}_{{\rm rel},p})^2 \rangle = \langle (k_p \Delta r_{{\rm rel},p}(\theta_p) \cos\theta_p)^2 \rangle = \alpha k^2 \langle \Delta r_{\rm rel}^2 \rangle /3$ is reduced by a numerical factor α, which measures the fraction of the relative mean square displacement of the particles detected by DAWS. For example, the factor α is reduced from 1 for uncorrelated motion to 0.6 for simple shear flow [14], while in the extreme case of a pure rotation, $\alpha = 0$, since the component of $\Delta\vec{r}_{{\rm rel},p}(\tau,l)$ parallel to the wave vector between adjacent scatterings is zero in this case [15]. By contrast, for the fluidized suspensions investigated in this paper, the motion is almost certainly uncorrelated over long measurement times; thus the magnitude of α is expected to be quite close to unity in this case, allowing us to use Eq. (8) directly. In general, as shown by Bicout and Maynard [15], this effect can be described quantitatively in terms of the temporal evolution of the strain tensor

$$\varepsilon_{ij}(\tau) = \frac{1}{2} \left(\frac{\partial u_i(\tau)}{\partial r_j} + \frac{\partial u_j(\tau)}{\partial r_i} \right) \tag{9}$$

that characterizes the local flow patterns. Here $\vec{u}(\tau) = \Delta\vec{r}(\tau)$ is the change in the position of the pth particle located at position $\vec{r}$, and i,j represent x, y, and z. By approximating the relative displacement of the particles by the leading term of a series expansion, we obtain

$$\Delta\vec{r}_{{\rm rel},p} = \Delta\vec{r}_{p+1} - \Delta\vec{r}_p \approx l(\hat{e}_p\cdot\nabla)\vec{u}, \tag{10}$$

where $\hat{e}_p = e_x^{(p)}\hat{i} + e_y^{(p)}\hat{j} + e_z^{(p)}\hat{k}$ is a unit vector in the direction of $\vec{k}_p$. The phase change $\Delta\phi_p(\tau)$ then becomes (ignoring the effect of the first and last scattering events)

$$\Delta\phi_p(\tau) = kl \sum_{i,j} e_i^{(p)} e_j^{(p)} \varepsilon_{ij}(\vec{r}_p,\tau). \tag{11}$$

Since for isotropic scattering the $\hat{e}_p$ are randomly distributed, $\langle \Delta\phi_p(\tau) \rangle$ is simply obtained by averaging each term in Eq. (11) over the unit sphere, giving

$$\langle \Delta\phi_p(\tau) \rangle = \frac{1}{3} kl \left\langle \sum_i \varepsilon_{ii} \right\rangle. \tag{12}$$

Thus, only the sum of the diagonal terms in the strain tensor survives in the ensemble average, showing that $\langle \Delta\phi_p(\tau) \rangle = 0$ unless there is a uniform dilation or compression of the entire sample. Therefore, as stated above, for incompressible media the decay of $g_1(\tau)$ is determined by $\langle \Delta\phi_p^2(\tau) \rangle$, which is now given by

$$\langle \Delta\phi_p^2(\tau)\rangle = \frac{2(kl)^2}{15}\left[\left\langle\left(\sum_i \varepsilon_{ii}\right)^2\right\rangle + 2\sum_{i,j}\langle\varepsilon_{ij}^2\rangle\right]. \quad (13)$$

The first term in Eq. (13) describes the effect of fluctuations in the density of the medium, due to local variations in the number of particles per unit volume, while the second term is simply the sum of all the mean square tensor strains. Thus the contribution to the relative mean square displacements of the particles that is measured in DAWS can be written in terms of the average strain $\overline{\varepsilon}$ as

$$\langle \Delta r_{\mathrm{rel,meas}}^2(\tau,l)\rangle = \overline{\varepsilon^2} l^2, \quad (14)$$

where

$$\overline{\varepsilon^2} \equiv \frac{2}{5}\left[\left\langle\left(\sum \varepsilon_{ii}\right)^2\right\rangle + 2\sum_{i,j}\langle\varepsilon_{ij}^2\rangle\right]. \quad (15)$$

To calculate $g_1(\tau)$ from a model for the strain field when the strains are inhomogeneously distributed throughout the sample volume, $\overline{\varepsilon^2}$ should also be weighted by the spatial distribution of diffusing sound in the medium for paths of length s [15].

When the scattering is anisotropic, so that $l^* > l_s$, all of the expressions for $g_1(\tau)$ in this section still hold providing that l is replaced everywhere by l^*. This result was first shown in DWS for particles undergoing random Brownian motion [9,10]; it has also been demonstrated more recently for particles in flows, so long as the strain and velocity fields vary slowly on the scale of the transport mean free path [17]. Thus, the field autocorrelation function can be written as

$$g_1(\tau) \approx \exp\left[-\frac{nk^2}{6}\langle \Delta r_{\mathrm{rel}}^2(\tau,l^*)\rangle\right] \quad (16)$$

or

$$g_1(\tau) \approx \exp\left[-\frac{nk^2 l^{*2}}{6}\overline{\varepsilon^2}(\tau,l^*)\right]. \quad (17)$$

Here the number of scattering events in the path, $n \approx s/l^* - 1 \approx s/l^* = v_e t_s / l^*$ is determined by the sampling time t_s, given by the corresponding time that the ultrasound has spent diffusing through the sample.

For suspensions of particles with dimensions comparable to the ultrasonic wavelength at megahertz frequencies, the Peclet number $\mathrm{Pe} \gg 1$, so Brownian motion is negligible and the motion of the particles is expected to be ballistic over short time intervals. Then $\Delta\vec{r}_p(\tau) = \vec{V}_p \tau$, and the relative mean square displacement $\langle \Delta r_{\mathrm{rel}}^2(\tau)\rangle = \langle \Delta V_{\mathrm{rel}}^2\rangle \tau^2$ provides a measure of the local variance in the relative velocity of the particles. In this regime, the strain is also proportional to t, so that the phase fluctuations $\langle \Delta\phi_p^2(\tau)\rangle$ can be conveniently expressed in terms of the strain rate tensor, $\gamma_{ij} = \varepsilon_{ij}/\tau = \frac{1}{2}(\partial V_i/\partial r_j + \partial V_j/\partial r_i)$ [15]. Thus, DAWS can also be used to measure the average local strain rate $\overline{\Gamma} = \overline{\varepsilon}/\tau \approx \Delta V_{\mathrm{rel}}/l^*$, where $\Delta V_{\mathrm{rel}} = \sqrt{\langle \Delta V_{\mathrm{rel}}^2\rangle}$.

Information on the spatial correlations of the particle motions can be obtained by varying the length scale l^* at which $\langle \Delta r_{\mathrm{rel}}^2(\tau)\rangle$ and $\langle \Delta V_{\mathrm{rel}}^2\rangle$ are measured. The relative mean square displacement of particles separated by l^* can be expressed as

$$\begin{aligned}\langle \Delta r_{\mathrm{rel}}^2(l^*)\rangle &= \langle[\Delta\vec{r}(l^*) - \Delta\vec{r}(0)]^2\rangle \\ &= 2\langle \Delta r^2\rangle - 2\langle \Delta\vec{r}(l^*)\cdot\Delta\vec{r}(0)\rangle. \end{aligned} \quad (18)$$

At early τ, where the motion is ballistic, this equation can be written in terms of the variance of the velocities as

$$\Delta V_{\mathrm{rel}}^2(l^*) = 2V_{\mathrm{rms}}^2\left[1 - \frac{\langle \vec{V}(0)\cdot\vec{V}(l^*)\rangle}{\langle |V(0)|^2\rangle}\right], \quad (19)$$

where V_{rms} is the root mean square velocity, which can be measured using dynamic sound scattering (DSS) [4]. Equation (19) shows that the length scale dependence of the relative mean square velocity of the particles is intimately related to the instantaneous spatial velocity correlation function $\langle \vec{V}(0)\cdot\vec{V}(l^*)\rangle / \langle |\vec{V}(0)|^2\rangle$, and that this correlation function can be probed by varying l^* in diffusing acoustic wave spectroscopy.

To calculate the correlation function $g_1^{(\mathrm{cw})}(\tau)$ for continuous-wave DAWS, we replace the sum in Eq. (4) by an integral over all path lengths s, where path length distribution function $P(s)$ is given by the solution of the diffusion equation, taking into account the appropriate boundary conditions and the effects of absorption [18]. For a slab-shaped sample cell with boundaries having an average reflectivity $\mathcal{R}$, $g_1^{(\mathrm{cw})}(\tau)$ in transmission is given by

$$g_1^{(\mathrm{cw})}(\tau) \simeq \int P(s)\exp\left[-\frac{s}{l^*}k^2\langle \Delta r_{\mathrm{rel}}^2(\tau)\rangle/6\right]ds = \frac{(L+2C)/(z_0+C)\{\sinh(z_0\sqrt{q^2+\alpha^2}) + C\sqrt{q^2+\alpha^2}\cosh(z_0\sqrt{q^2+\alpha^2})\}}{[1+C^2(q^2+\alpha^2)]\sinh(L\sqrt{q^2+\alpha^2}) + 2C\sqrt{q^2+\alpha^2}\cosh(L\sqrt{q^2+\alpha^2})}, \quad (20)$$

where $q^2 = k^2\langle \Delta r_{\mathrm{rel}}^2(\tau)\rangle/2l^{*2}$, $\alpha^2 = 1/D\tau_a$, τ_a is the absorption time, $z_0 \sim l^*$ is the distance inside the sample where sound diffusion "begins," and $C = \frac{2}{3}l^*(1+\mathcal{R})/(1-\mathcal{R})$. Thus, inverting $g_1^{(\mathrm{cw})}(\tau)$ to determine the motion of the scatterers is more complicated for cw DAWS, and requires a more complete description of the diffusive propagation of sound through the sample.

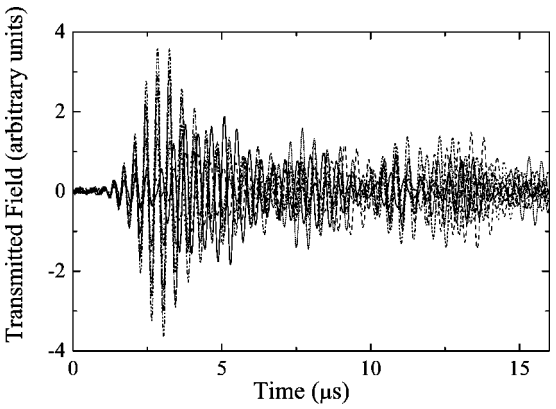

FIG. 2. Sequence of transmitted wave forms, consisting of waves that have been multiply scattered in the sample after a 1-μs-wide input pulse is incident on the front face of the sample. The input pulse is centered at $t=0$ s. As the time for the multiply scattered waves to travel through the sample increases and the scattered path lengths become longer, the rate at which the scattered field becomes decorrelated on subsequent pulse repetitions increases.

III. EXPERIMENT

To demonstrate how DAWS can be realized experimentally, fluidized beds were constructed in which 0.875-mm-diameter glass beads were suspended in a mixture of 75% glycerol and 25% water [4,5]. The liquid was pumped upwards at a constant velocity V_f to counterbalance the gravitational sedimentation of the beads, different values of V_f being selected to vary the volume fraction of the particles between 0.08 and 0.50. For this choice of glass bead diameter and liquid viscosity, the particle Reynolds number, $\mathrm{Re}_p = 2a\rho_f V_0/\eta$, ranges from 0.3 at 23 °C to 0.9 at 27 °C. Here ρ_f and η are the fluid density and viscosity, respectively, a is the particle radius, and V_0 is the Stokes velocity. In this paper, we show representative results obtained using several different fluidized beds, although most of the data were taken in a bed with height, width, and thickness of 450, 178, and 12.8 mm, respectively. Uniform flow at the bottom of the beds was established using a distributor of close-packed stationary beads.

The majority of our measurements of the temporal correlation function were performed using pulsed techniques, thereby taking advantage of the higher power levels and better signal-to-noise characteristics of pulsed ultrasonic experiments relative to cw methods. We used a transmission geometry, in which the incident pulse was an excellent approximation to a plane wave over the cross section of the sample, and the transmitted multiply scattered field was detected in a single (near-field) speckle using a miniature hydrophone [7]. For pulsed measurements, the full time dependence of the scattered field transmitted through the sample after each incident pulse can, in principle, be measured, giving a series of time-domain pictures of the scattered field wave form, recorded at each repetition of the incident pulse. As an illustrative example, we show in Fig. 2 a sequence of transmitted wave forms taken in the fluidized bed. The carrier frequency in the pulse was centered at $f=2.3$ MHz, where the ultrasonic wavelength λ is comparable to the particle radius a, and strong multiple scattering is evident from the long range of transit times taken by the input pulse to reach the detector. Since the scattering particles are moving, the wave form changes with each subsequent acquisition of the scattered field, allowing their dynamics to be probed on a time scale determined by the inverse of the pulse repetition frequency. In this example, the pulse repetition rate was 100 ms, allowing the fluctuations in the transmitted field to be easily seen, and showing clearly that the fluctuation rate increases with transit time through the sample as the multiple scattering paths become longer. This figure shows graphically how the sensitivity of the measurements to small motions of the scatterers can be controlled by selecting the sampling time and hence the path length—the longer the path, the greater the sensitivity to small displacements of the particles, since the sound scatters more times before leaving the sample and each scattering particle has to move a smaller fraction of a wavelength to achieve the same accumulated phase change of the scattered field.

To optimize the rate at which the fluctuations can be probed in pulsed DAWS, it is advantageous to measure the field fluctuations at a single sampling time t_s after the input pulse is incident on the sample, rather than to digitize the entire wave form. This is achieved by using a boxcar integrator to sample the scattered field over a very narrow time interval, chosen to be much less than the ultrasonic period so that the true field at this instant is accurately measured. The sampled field at this point on the wave form is then digitized for each repetition of the pulse using the gated digitizing option of a PC oscilloscope card. In these measurements, it is critical to synchronize the acquisition rate of the oscilloscope to the pulse repetition frequency, and the use of gated digitizing was found to be more reliable than attempting to synchronize the time base of the digital oscilloscope and the pulse repetition period. The use of the boxcar dramatically increases the rate at which data can be acquired in successive repetitions of the pulse, and allows the temporal fluctuations of the scattered field to be sampled at times separated by values that approach the fundamental limit imposed by the time taken for sound to diffuse across the sample, typically 50–100 μs in the current experiments. Although this method does not allow the amplitude and phase of the scattered fields to be independently determined, it does allow the field correlation function to be calculated directly from the oscilloscope data. Since any point on the scattered wave form can be selected by shifting the gate position on the boxcar integrator, the main advantages of pulsed diffusing acoustic wave spectroscopy can all be realized with this relatively simple technique.

Typical results using this method are shown in Fig. 3. In Fig. 3(a), a single snapshot of the transmitted field is shown and compared with the input pulse. Two sampling times t_s at which the field is measured by the boxcar on subsequent repetitions of the input pulse are shown by the vertical arrows. By using a pulse repetition frequency of 1 kHz, the field fluctuations $\psi(t)$ were measured every millisecond, giving the results shown in Fig. 3(b), where the fluctuations at these two sampling times are compared over a 2-s time in-

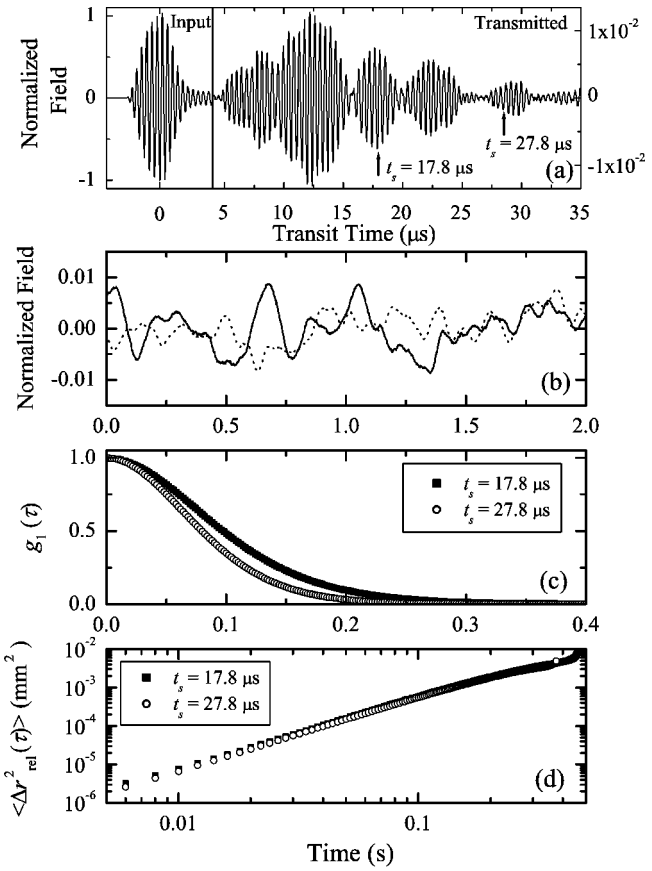

FIG. 3. (a) Input (left) and transmitted (right) pulses. The vertical arrows indicate two different times at which the field is sampled. The fields are normalized so that the peak value of the input pulse is equal to 1. (b) The field fluctuations measured at these two sampling times. The solid curve corresponds to $t_s = 17.8$ μs, while the dashed curve corresponds to $t_s = 27.8$ μs. (c) The field autocorrelation functions calculated from the field fluctuations. (d) The relative mean square displacements of the particles as a function of time.

terval. Generally, a sequence of 131 000 pulses was used, allowing the variation in the field $\psi(t)$ to be followed over ≈ 2 min, long enough to have sufficiently good statistics to determine the correlation function with excellent sensitivity. The temporal autocorrelation functions of $\psi(t)$ were calculated from the digitized field fluctuations using fast Fourier transforms (FFT) and the correlation theorem, which states that the Fourier transform of an autocorrelation function is equal to the product of the Fourier transform of the function and its complex conjugate [19]. For long record lengths, this FFT method is much less computationally intensive than the brute force calculation using the relation

$$g_1(\tau) = \frac{\int \psi(t)\psi^*(t+\tau)dt}{\int |\psi(t)|^2 dt} \approx \frac{\frac{1}{n-j}\sum_{i=1}^{n-j} \psi(t_i)\psi^*(t_i-\tau_j)}{\frac{1}{n}\sum_{i=1}^{n} |\psi(t_i)|^2}. \tag{21}$$

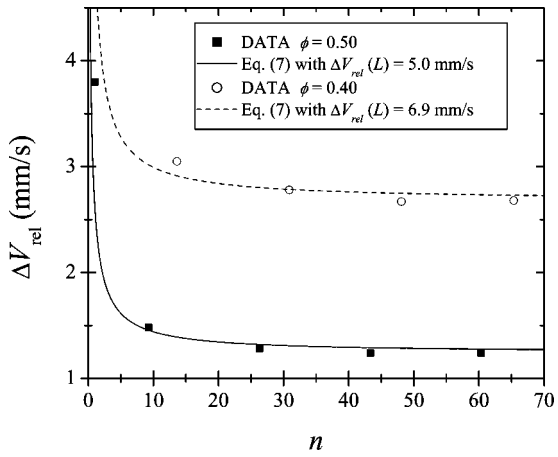

FIG. 4. The rms relative velocity determined from the experimental data using Eq. (16) as a function of the number of scattering events n (symbols). The curves represent the sum of the actual rms relative velocity, as measured from long path lengths, plus the correction term given in Eq. (7), which is fitted to the experimental data thereby determining $\langle \Delta V^2_{\rm rel}(R) \rangle$.

Note that these measurements give the field autocorrelation function $g_1(\tau)$ directly. To further improve the statistics, this procedure was repeated 50 times and the resulting correlation functions then averaged together. Results for $g_1(\tau)$ at the two sampling times selected in Figs. 3(a) and 3(b) are shown in Fig. 3(c), indicating that the correlation function decays more quickly for the longer path lengths probed at the larger sampling time, as expected from Eq. (16).

To determine $\langle \Delta r^2_{\rm rel}(\tau) \rangle$ or $\overline{\varepsilon^2}(\tau)$ from $g_1(\tau)$, the parameters $s = v_e t_s$, l^*, and k must be determined from measurements of the diffusive and ballistic transport of ultrasound through the sample [7,8,20–22]. For suspensions of solid particles in a fluid, we have shown that it is a good approximation to take $v_e \approx v_g$ and $l^* \approx l_s$, so that a first-order estimate of the required ultrasonic propagation parameters can be obtained from ballistic measurements of the scattering mean free path l_s, the phase velocity v_p $(= 2\pi f/k)$, and the group velocity v_g. More accurate results can be obtained by measuring D and l^* directly from pulsed and cw experiments on the diffusive propagation of ultrasound through the sample, using the methods described in Ref. [7]. Using the values of v_e, l^*, and k determined in these experiments, we use Eq. (16) to invert the correlation functions in Fig. 3(c) and determine the time dependence of $\langle \Delta r^2_{\rm rel}(\tau) \rangle$, as shown in Fig. 3(d). Note that the data taken at the two different sampling times give essentially the same values of $\langle \Delta r^2_{\rm rel}(\tau) \rangle$, demonstrating that the dependence on path length is correctly described by our model for the correlation function.

To explore the path length dependence in more detail, we have taken measurements at several different sampling times or path lengths. By comparing the relative mean square displacements calculated from our data using Eq. (16), we can test whether the correction term introduced by the first and last scattering events is negligible. In Fig. 4, the relative mean square velocities extracted from these data sets are plotted versus the number of scattering events, for samples

with two different volume fractions. For $n>20$ the differences caused by the $1/n$ correction term in Eq. (7) are small and not significant when compared to other sources of uncertainty (e.g., in the transport mean free path and energy velocity). However, as n gets smaller, the influence of the correction term becomes evident. To investigate the magnitude of the correction term, we fit the form expected from Eq. (7), treating $\langle \Delta V_{\rm rel}^2(R)\rangle = \langle \Delta r_{\rm rel}^2(R)\rangle / \tau^2$ as the unknown, to obtain the solid and dashed curves in Fig. 4. As an example of the results of these fits, we find for the 50% volume fraction data, that the fitted value of $\Delta V_{\rm rel}(R)$ is 5.0 mm/s; this value is between our independent measurements, using DAWS and DSS, of $\Delta V_{\rm rel}=3.1$ mm/s at a separation equal to the sample thickness of 5.4 mm, and $\Delta V_{\rm rel}=\sqrt{2}V_{\rm rms}=7.6$ mm/s at separations larger than the correlation length ($\xi=22$ mm). Thus, the value of $\Delta V_{\rm rel}(R)$ extracted from the fit is reasonable, since the average distance between the first and last scattering events should be somewhat larger than the sample thickness. It should be noted that these results imply that pulsed DAWS can be used on samples whose thickness is less than the four mean free paths that are needed for the diffusion approximation to accurately determine the distribution of path lengths [24]. One need only set the sampling time, or equivalently the path length, to be long enough that the detected ultrasound has undergone more than 20 scattering events. This is in contrast to the situation with continuous wave DAWS or DWS, where in order to examine thin samples one must go beyond the diffusion approximation, for example, by using radiative transfer theory or the telegrapher equation, to take the short paths into account [25,26].

We have also investigated the relative motion of the scattering particles using continuous waves instead of pulses, a method that is similar in many respects to that usually employed in diffusing wave spectroscopy with light. The potential advantages of cw DAWS are twofold: first, the ultrasonic waves are monochromatic, thus avoiding possible complications in the analysis in cases where the ultrasonic mean free path or energy velocity are strongly frequency dependent, and second, it is possible to measure faster dynamics, since the fluctuations can be measured continuously without waiting for the next pulse to propagate through the sample. However, these advantages are often outweighed by the increased complexity of the correlation function in cw DAWS, limiting its usefulness to those cases where fast dynamics or very large ultrasonic dispersion makes pulsed techniques less reliable. To directly measure the field fluctuations in cw DAWS, the boxcar is phase locked so that the scattered field is measured at regular time intervals that are exact multiples of the period of the input wave. Thus the true fluctuations of the field, due to the combined effects of the fluctuations in amplitude and phase, are measured without the trivial contribution due to the $\exp(i\omega t)$ oscillations of the carrier wave. Having measured the field fluctuations, the cw field autocorrelation function is determined using the same FFT method described above for pulsed DAWS.

By determining $g_1^{(\rm cw)}(\tau)$ for these data, and solving for $\langle \Delta r_{\rm rel}^2(\tau)\rangle$ using Eq. (20), we can compare the values of the relative mean square displacements obtained from cw and pulsed DAWS. Our results are shown in Fig. 5, where the cw and pulsed data are represented by the solid and open symbols, respectively. Note the increased sensitivity of the cw data to the early time motion. Good agreement between the two methods is found, especially for times between 10^{-3} and 10^{-2} s, where they give essentially the same rms velocity. At later times the agreement is not as good, most likely due to the increased contributions to the cw autocorrelation function of short paths through the sample at large correlation times (g_1 decays more slowly for short paths than for longer paths), since these paths are not as well modeled by the diffusion approximation [25]. Nonetheless, continuous-wave DAWS allows for the measurement of faster particle dynamics than pulsed techniques, and gives accurate results of the relative mean square displacements at short times where this technique is most needed.

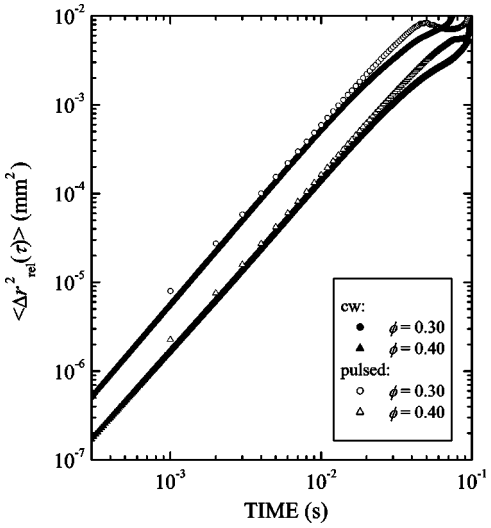

FIG. 5. Comparison of pulsed (open symbols) and cw (closed symbols) DAWS measurements of the relative mean square displacement at two different volume fractions.

IV. RESULTS AND DISCUSSION

Figure 6 shows typical results for the variance of relative mean square particle displacements measured by DAWS in fluidized suspensions. Here we show the time dependence of $\langle \Delta r_{\rm rel}^2(\tau)\rangle$ for several volume fractions in two cells having different thicknesses. The data for the two cells are in excellent agreement, except for the data at $\phi=0.40$, where the difference in $\langle \Delta r_{\rm rel}^2(\tau)\rangle$ can be entirely accounted for by a measured difference in temperature. These measurements were performed at a frequency of 2.35 MHz, for which the ultrasonic wavelength λ in the suspension varied slightly from 0.68 to 0.75 mm as the volume fraction ϕ was increased from 0.18 to 0.50. Note the range of distances probed by this technique: these range from $\approx\lambda/2$ down to $\lambda/1000$ at the earliest times, illustrating the extremely good sensitivity of DAWS to small relative displacements of the particles. At early times $\langle \Delta r_{\rm rel}^2(\tau)\rangle$ varies quadratically with time, as expected when the particles move in ballistic trajec-

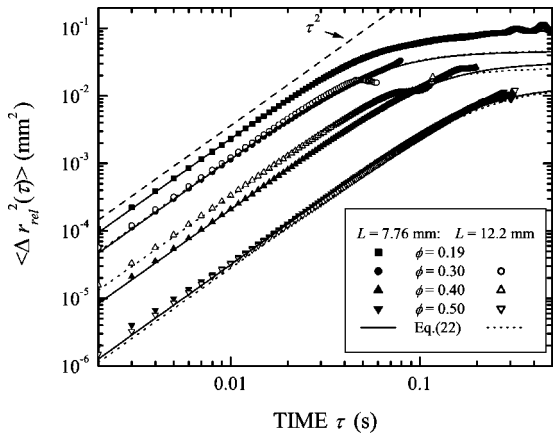

FIG. 6. Mean square displacement of the beads relative to their neighbors at several volume fractions ϕ, along with fits of the phenomenological function given by Eq. (22) to the data.

tories with relative velocity $\Delta\vec{V}_{\rm rel}$. At later times, however, the relative mean square displacement varies less strongly with time, becoming approximately independent of time at the longest times measured, as the particle trajectories become influenced by their neighbors. We represent this behavior by the phenomenological expression

$$\langle \Delta r_{\rm rel}^2(\tau)\rangle = \frac{\langle \Delta V_{\rm rel}^2\rangle \tau^2}{1+(\tau/\tau_{cl})^2}, \tag{22}$$

where τ_{cl} is the local crossover time, or the average time interval after which the ballistic motion is altered by interparticle interactions. Fits of this empirical expression to our data are shown by the solid curves in Fig. 6. This figure shows that Eq. (22) gives an excellent description of the crossover behavior, allowing accurate measurements of both $\Delta V_{\rm rel}=\sqrt{\langle \Delta V_{\rm rel}^2\rangle}$ and τ_{cl} to be obtained.

In Sec. II, we emphasized that DAWS measures $\langle \Delta r_{\rm rel}^2(\tau)\rangle$ on a length scale determined by the ultrasonic transport mean free path l^*. In Fig. 7, we plot the values of l^* as a function of volume fraction for the measurements of

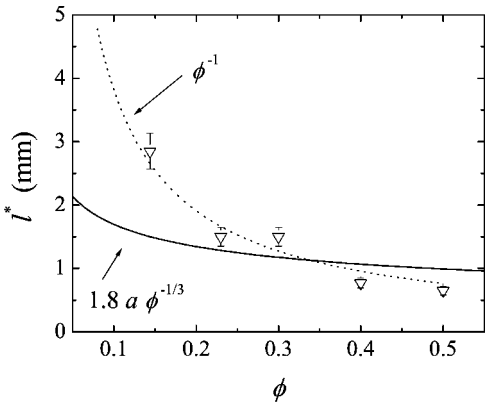

FIG. 7. The smallest values of the transport mean free path l^* used in our experiments, performed at a frequency of 2.35 MHz. These data are compared with the average nearest-neighbor distance between the particles.

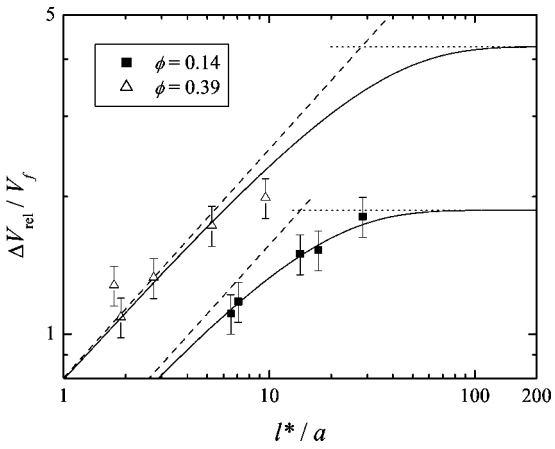

FIG. 8. The rms relative velocity, normalized by the fluidization velocity, as a function of l^*/a, which determines the average particle separation (in units of the particle radius a) at which $\Delta V_{\rm rel}$ is measured. Experimental results for two volume fractions are shown (symbols) along with fits of Eq. (23) to the data (solid curves). The dotted horizontal lines represent the rms velocity of the particles measured using dynamic sound scattering, and the dashed lines show the $\sqrt{l^*/a}$ dependence seen at small particle separations.

$\langle \Delta r_{\rm rel}^2(\tau)\rangle$ shown in Fig. 6 [27]. As expected, l^* varies as ϕ^{-1} [21,28]. These measurements of l^* are also compared with the average center-to-center distance between nearest-neighbor particles in the suspension, which is given approximately by $d_{nn}=1.8a\,\phi^{-1/3}$ since d_{nn} is equal to $2a$ for close packing. At this ultrasonic frequency ($f=2.35$ MHz), l^* is similar in magnitude to d_{nn} throughout the entire range of volume fractions, demonstrating the very short length scales at which the relative motion of the scattering particles can be measured in DAWS.

By lowering the ultrasonic frequency below $f=2.35$ MHz, we are able to investigate the dependence of the relative velocity fluctuations on length scale, since l^* increases at lower frequencies as the wavelength becomes larger than the particle size. As discussed in Sec. II [see Eq. (19)], varying l^* allows us to probe the instantaneous spatial correlations of the particle velocities, since we can measure $\Delta V_{\rm rel}$ at early times before the correlations have begun to decay temporally. Typical data for two different volume fractions are illustrated in Fig. 8, which shows $\Delta V_{\rm rel}$, normalized by the average fluid flow velocity V_f, as a function of l^*, normalized by the bead radius. Also shown, by the dotted horizontal lines, is $\sqrt{2}$ times the root mean square velocity $V_{\rm rms}$, measured using DSS, and again normalized by the fluid flow velocity V_f. At small particle separations, $\Delta V_{\rm rel}$ is proportional to the square root of the average interparticle separation l^*, giving a direct measure of the correlations in the particle velocities. At larger particle separations the velocity correlations weaken, and the relative velocity of the particles approaches $\sqrt{2}V_{\rm rms}$, the value expected for particles that move randomly. This behavior is well described by Eq. (19) if we assume that the velocity correlation function decays exponentially with distance, so that

$$\frac{\Delta V_{\rm rel}}{\Delta V_{\rm rms}} = \sqrt{2}[1-\exp(-l^*/\xi)]^{1/2}, \tag{23}$$

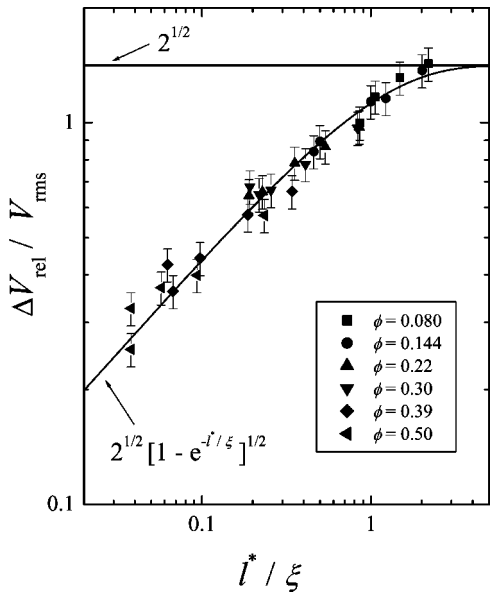

FIG. 9. The relative velocity, normalized by the rms velocity, plotted as a function of the particle separation, normalized by the measured correlation length. Data from all the samples fall onto the same curve, governed by an exponentially decaying correlation function [Eq. (23)].

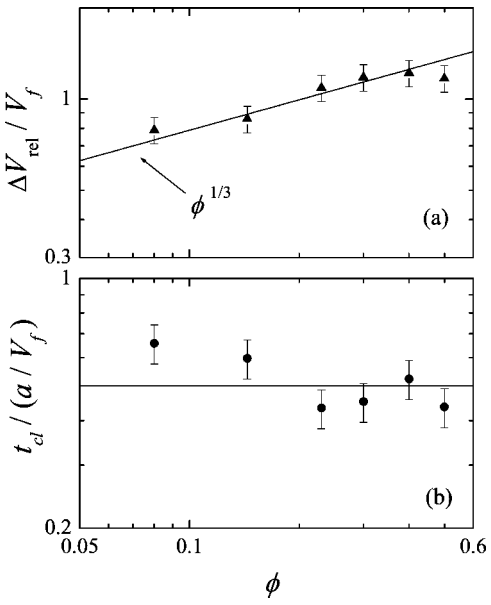

FIG. 10. (a) The root mean square relative velocity at the nearest-neighbor separation, normalized by the fluid flow velocity and plotted as a function of volume fraction for three different sample thicknesses. The solid line shows the $\phi^{-1/3}$ dependence exhibited by the data up to a volume fraction of about 0.4. (b) The local crossover time τ_{cl} divided by the time for the fluid to travel a single bead radius, a/V_f. The horizontal line shows that the normalized crossover time is ≈ 0.5.

where ξ is the instantaneous velocity correlation length. The solid lines in Fig. 8 show the results of fitting of Eq. (19) to the data with only a single fitting parameter, namely, the correlation length ξ, whose magnitude can then be determined. Note that both the $\sqrt{l^*}$ behavior seen in our data at short length scales and the crossover to a relative velocity that is independent of length scale at longer length scales, are well characterized by Eq. (23). Thus, by combining measurements of the relative velocity as a function of length scale using DAWS with measurements of the rms velocity using DSS, we are able to determine the spatial extent of the correlations in the particles' motion and indirectly measure the velocity correlation function.

To further demonstrate that the length scale dependence of the relative velocity fluctuations is well described by Eq. (23), Fig. 9 shows our data for all the volume fractions investigated in the $450 \times 178 \times 12.8$ mm^3 cell. In this figure, we normalize the relative velocity for each volume fraction by the corresponding value of $V_{\rm rms}$, and the average particle separation by the measured correlation length ξ. Remarkably, all the data collapse onto a single curve, which is given by Eq. (23) for effective particle separations spanning nearly two orders of magnitude. This scaling plot indicates that the velocity correlation function decays exponentially with distance over the entire range of particle separations investigated, allowing the velocity correlation length to be reliably measured from the length scale dependence of $\Delta V_{\rm rel}$.

Furthermore, by using the $\sqrt{l^*}$ dependence of the relative velocity to interpolate or extrapolate $\Delta V_{\rm rel}$ to the nearest-neighbor particle separation, we measure the local relative velocity at the shortest distances over which the relative motion can be defined. Figure 10(a) shows the local relative velocity, normalized by fluid velocity V_f, as a function of volume fraction. As in Fig. 9, these data were taken in one of our cells that is about 30 bead radii thick. Figure 10(a) shows that the relative velocity is large, even at this shortest length scale, and increases approximately as $\phi^{1/3}$ up to a volume fraction of 0.40. At higher ϕ, $\Delta V_{\rm rel}$ starts to decrease again as the particle flows become more strongly correlated. The second quantity that can be directly measured from the time dependence of $\langle \Delta r_{\rm rel}^2(\tau) \rangle$ is the local crossover time τ_{cl}, which we plot in Fig. 10(b) as a function of the volume fraction. Here we have normalized τ_{cl} by the characteristic time taken by the fluid to travel a bead radius, $t_f = a/V_f$. This figure shows that the ratio $\tau_{cl}/t_f \approx 1/2$ throughout the entire volume fraction range; thus, the particles move ballistically relative to each other for quite short times during which the fluid has, on average, only moved a distance equal to one half the particle radius. These results for τ_{cl} also allow us to determine a length scale for local motions in fluidized suspensions, $\Delta d_{\rm sep} = \Delta V_{\rm rel} \tau_{cl} / \sqrt{3}$; this length scale corresponds to the average change in the separation of adjacent particles before their trajectories become modified by interparticle interactions, and is typically about one-fourth of the particle radius.

These results for the local relative velocity also allow us to measure the average strain rate $\overline{\Gamma}$ at the average nearest-neighbor separation, as shown by the solid symbols in Fig. 11(a). Again we normalize $\overline{\Gamma}$ by $t_f = a/V_f$, thereby accounting for the fact that the fluidization velocity sets the scale for the strain rate as well as for the velocity fluctuations. Figure 11(a) shows that the local strain rate is large, indicating that there are very considerable local rearrangements of the par-

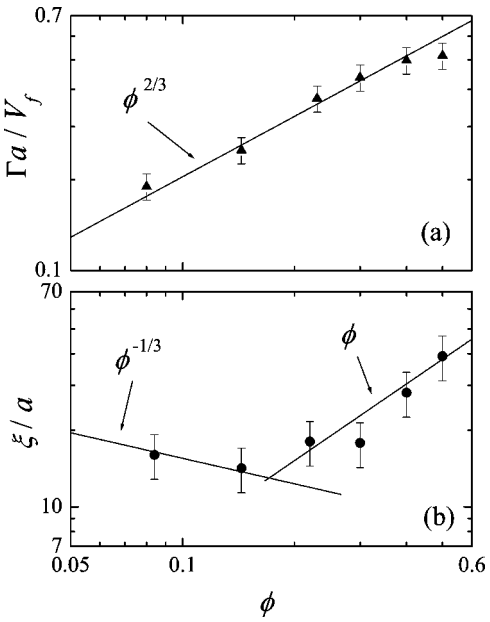

FIG. 11. (a) The local average strain rate at the nearest-neighbor separation, normalized by a/V_f. (b) The instantaneous correlation length, normalized by the particle radius, measured using DAWS and DSS, and plotted versus volume fraction for two sample thicknesses. The lines are power law fits to the data.

ticles over short times. Physically, since $t_f \approx 2\tau_{cl}$ [c.f., Fig. 10(b)], the normalized strain rate $\overline{\Gamma} a/V_f$ corresponds to roughly twice the maximum strain that any local cluster of nearest-neighbor particles experiences before each particle's direction of motion is altered. At low volume fractions, the normalized strain rate at the nearest-neighbor separation increases more rapidly with ϕ than the relative velocity, reflecting decrease in particle separation with volume fraction. Up to $\phi \approx 0.4$, $\overline{\Gamma} a/V_f$ varies $\approx \phi^{2/3}$, but it eventually drops off at even higher volume fractions as the confining effect of the neighboring particles causes the flows to become more correlated.

Finally, we show in Fig. 11(b) how the instantaneous correlation length varies with volume fraction for the same fluidized bed with thickness $30a$. At low volume fractions ($\phi < 0.2$) we find a $\approx \phi^{-1/3}$ dependence on volume fraction, which means that the number of particles in a correlation volume remains approximately constant at different volume fractions. At these low volume fractions, the magnitude and volume fraction dependence of our data are in agreement with the extrapolation of particle imaging velocimetry experiments on sedimenting suspensions [30], measured at very low volume fractions and a much lower particle Reynolds number. At high volume fractions, however, the correlation length increases quite rapidly with ϕ, exhibiting an approximately linear dependence on volume fraction. This dependence has the interesting and somewhat surprising consequence that the number of particles in a correlation volume increases with volume fraction as ϕ^4, so that the correlation volume contains about 40 times more particles at $\phi = 0.5$ than it does at $\phi = 0.2$.

V. CONCLUSIONS

By taking advantage of recent progress in understanding the diffusive propagation of ultrasound in strongly scattering media, we have developed the ultrasonic technique called diffusing acoustic wave spectroscopy (DAWS). This technique uses multiply scattered ultrasonic waves to investigate the dynamics of systems in which traditional imaging techniques break down and other approaches are needed to investigate their properties. In this paper, we describe both the theoretical foundations and practical implementation of DAWS. As an example of the possible applications of this technique, we show how it can be used to study the complex flow behavior of particulate suspensions, focusing on fluidized suspensions of millimeter-sized particles in a liquid. In this type of system, DAWS gives a sensitive approach for measuring both the relative motion of the scatterers and the strain rate over a wide range of length scales, down to the distance between nearest-neighbor particles. In addition, DAWS can measure the time interval τ_{cl} before interparticle interactions modify the relative trajectories of the particles, giving information on the local length scale of the particle dynamics Δd_{sep}, which is equal to the average change in the separation between nearest-neighbor particles during τ_{cl}. Since DAWS measures the relative motion of the scatterers over a range of length scales, it also probes the spatial correlations of the particle velocities; when combined with measurements of the rms particle velocity using dynamic sound scattering, we have shown how DAWS can be used to measure the velocity correlation function and hence determine the velocity correlation length ξ. These data for fluidized suspensions demonstrate the considerable potential of this technique for determining important information about the dynamics of strongly scattering materials, information that can be used both in fundamental studies of their dynamic properties as well as in practical applications in the nondestructive characterization of materials.

ACKNOWLEDGMENTS

We wish to acknowledge NSERC, NATO, and the donors of the Petroleum Research Fund, administered by the ACS, for support of this research. We would also like to thank Arthur E. Bailey for his assistance with some of our initial experiments.

[1] L. C. Lynnworth, *Ultrasonic Measurements for Process Control* (Academic Press, New York, 1989).

[2] A. Briggs, *An Introduction to Scanning Acoustic Microscopy* (Oxford University Press, Oxford, 1985).

[3] D. H. Evans, *Doppler Ultrasound: Physics, Instrumentation, and Clinical Applications* (Wiley, New York, 1989).

[4] M.L. Cowan, J.H. Page, and D.A. Weitz, Phys. Rev. Lett. **85**, 453 (2000).

[5] J.H. Page, M.L. Cowan, and D.A. Weitz, Physica B **279**, 130 (2000).
[6] J. H. Page, M. L. Cowan, P. Sheng, and D. A. Weitz, in *IUTAM Symposium 99/4: Mechanical and Electromagnetic Waves in Structured Media*, edited by R. C. McPhedran, L. C. Botten, and N. A. Nicorovici (Kluwer Academic, Dordrecht, 2001), p. 121.
[7] J.H. Page, H.P. Schriemer, A.E. Bailey, and D.A. Weitz, Phys. Rev. E **52**, 3106 (1995).
[8] H.P. Schriemer, M.L. Cowan, J.H. Page, P. Sheng, Z. Liu, and D.A. Weitz, Phys. Rev. Lett. **79**, 3166 (1997).
[9] G. Maret and P.E. Wolf, Z. Phys. B: Condens. Matter **65**, 409 (1987).
[10] D.J. Pine, D.A. Weitz, P.M. Chaikin, and E. Herbolzheimer, Phys. Rev. Lett. **60**, 1134 (1988).
[11] D. A. Weitz and D. J. Pine, in *Dynamic Light Scattering*, edited by W. Brown (Clarendon, Press, Oxford, 1993), p. 652.
[12] T.G. Mason and D.A. Weitz, Phys. Rev. Lett. **74**, 1250 (1995).
[13] Incident sound penetrates an average distance l into the sample before the first scattering event occurs, and similarly travels an average distance l before leaving the sample after the last scattering event. Thus, for n scattering events, the total average path length s through the sample is the sum of the distance between the first and last scatterers, $(n-1)l$, and the distance $2l$ traveled inside the sample before the first and after the last scattering events, giving $s=(n+1)l$.
[14] To determine α for a simple shear flow with a velocity profile $V_x=\Gamma z\hat{e}_x$, we use Eq. (13) to write the field autocorrelation function in terms of the strain rate $\Gamma=\partial V_x/\partial z$ as $g_1(\tau) \simeq \exp(-nk^2l^2\Gamma^2\tau^2/15)$ [16,17]. Thus, the factor α is given by $\alpha=\frac{2}{5}l^2\Gamma^2\tau^2/\langle\Delta r_{rel}^2(\tau,l)\rangle$. $\langle\Delta r_{rel}^2(\tau,l)\rangle$ is found by averaging $\Delta r_{rel}^2(\tau,r)=r^2\cos^2\theta\Gamma^2\tau^2$ weighted by the probability that a scattered wave travels a distance r in any direction before being scattered again, this probability being given by $P(r,\theta,\phi)dr\,d\theta\,d\phi=(1/l)\exp(-r/l)dr\sin\theta\,d\theta\,d\phi/4\pi$. Hence, $\langle\Delta r_{rel}^2(\tau,l)\rangle=\frac{2}{3}l^2\Gamma^2\tau^2$, giving $\alpha=0.6$.
[15] D. Bicout and R. Maynard, Physica A **199**, 387 (1993).
[16] X-L. Wu, D.J. Pine, P.M. Chaikin, J.S. Huang, and D.A. Weitz, J. Opt. Soc. Am. B **7**, 15 (1990).
[17] D. Bicout and G. Maret, Physica A **210**, 87 (1994).
[18] J.X. Zhu, D.J. Pine, and D.A. Weitz, Phys. Rev. A **44**, 3948 (1991).
[19] W. H. Press, S. A. Teukolsky, W. T. Vetterling, and B. P. Flannery, *Numerical Recipes* (Cambridge University Press, Cambridge, 1992).
[20] J.H. Page, P. Sheng, H.P. Schriemer, I. Jones, X. Jing, and D.A. Weitz, Science **271**, 634 (1996).
[21] M.L. Cowan, K. Beaty, J.H. Page, Z. Liu, and P. Sheng, Phys. Rev. E **58**, 6626 (1998).
[22] An alternative approach for measuring both the diffusion coefficient and the transport mean free path is to use time-dependent coherent backscattering [23].
[23] A. Tourin, A. Derode, P. Roux, B.A. van Tiggelen, and M. Fink, Phys. Rev. Lett. **79**, 3637 (1997).
[24] Z.Q. Zhang, I.P. Jones, H.P. Schriemer, J.H. Page, D.A. Weitz, and P. Sheng, Phys. Rev. E **60**, 4843 (1999).
[25] F.C. MacKintosh and S. John, Phys. Rev. B **40**, 2383 (1989).
[26] P.-A. Lemieux, M.U. Vera, and D.J. Durian, Phys. Rev. E **57**, 4498 (1998).
[27] As indicated in Sec. III, l^* can be measured directly either by measuring the absolute transmission [7] or the coherent backscattering cone [23]. However, for the results shown in Fig. 7, we used a simpler, but nonetheless accurate, approach. We first measured the scattering mean free path l_s, which (in the absence of absorption) is the exponential decay length of the coherent, ballistic intensity [20,21]. The transport mean free path l^* was then determined from l_s using the relationship [28] $l^*=l_s/(1-\langle\cos\theta\rangle)$. Here $\langle\cos\theta\rangle=\int|f(\theta)|^2\cos\theta d\Omega/\int|f(\theta)|^2d\Omega$ was calculated from the angular dependence of the scattering amplitude $f(\theta)$ using the spectral function approach [29], which has been shown to give an accurate description of wave transport in this system [8,20,21].
[28] A. Lagendijk and B.A. van Tiggelen, Phys. Rep. **270**, 143 (1996).
[29] X. Jing, P. Sheng, and M. Zhou, Phys. Rev. A **46**, 6513 (1992).
[30] P.N. Segrè, E. Herbolzheimer, and P.M. Chaikin, Phys. Rev. Lett. **79**, 2574 (1997).